

A simple model for dense phases of two-dimensional hard rods and its application to mono- and bidisperse alkanes physisorbed on graphite

R. Hentschke, L. Askadskaya, and J. P. Rabe
Max-Planck-Institut für Polymerforschung, Postfach 3148, W-6500 Mainz, Germany

(Received 14 April 1992; accepted 28 July 1992)

Based on a simple mean field model, we study the positional ordering in dense systems of mono- and bidisperse parallel hard rods in two dimensions. We obtain phase diagrams exhibiting nematic, columnar, and crystalline order as a function of the packing density, the lengths, and the mixing ratio of the particles. Even though our theory neglects the details of the molecular interactions, it proves to be applicable to physisorption of large anisotropic molecules on smooth surfaces. This is demonstrated on the basis of scanning tunneling microscopy experiments on dense monolayers of highly ordered alkane chains physisorbed on graphite. Crystalline as well as columnar orderings are observed as a function of molecular weight for monodisperse adsorbates and, in addition, in terms of the mixing ratio for bidisperse adsorbates, in accord with the predictions of the model.

INTRODUCTION

Hard particle excluded volume theories are often reasonable models for the description of liquid crystalline behavior in systems of large anisotropic molecules or molecular aggregates. Since Onsager's seminal work on the isotropic-to-nematic transition in systems of hard rigid rods,¹ a large body of work has been added using various mostly approximate methods to include lyotropic phase behavior at high densities, where both orientational and translational order may occur, systems of more complicated composition, particles of more complex geometry or particles possessing flexibility (cf. the review articles in Refs. 2, 3, 4, 5, and references therein). One such approach was recently proposed by Taylor, Hentschke, and Herzfeld^{6,7} to study the complex translational ordering of monodisperse hard spherocylinders. Their method is based on an approximate separation of the nonideal part of the free energy into contributions describing the translationally disordered (fluidlike) and translationally ordered (crystal-like) dimensions occurring in a particular phase. This concept is straightforwardly applicable in a variety of real systems, like lyotropic chain polymers or aggregates of reversibly assembling amphiphiles. The major shortcoming of the model is that the dimensional separation of the free energy imposes stringent positional constraints which force all transitions to be discontinuous. However, the model's intuitiveness and its predictive quality regarding rather complex phase topologies, e.g., nematic, columnar, smectic, and crystalline ordering as a function of density, particle geometry, persistence length, and aggregation energy, make it a valuable tool.

In this work, we discuss the application of the above model to mono- and bidisperse systems of hard rods confined to a plane, i.e., rods in two dimensions. We calculate phase diagrams for these systems in terms of the (surface) packing density, the aspect ratio of the rods, and, in the bidisperse case, the mixing ratio, i.e., the ratio of the number of long rods to the number of short rods. We also show

that the results are applicable to positionally ordered phases occurring in systems of large anisotropic molecules physisorbed on atomically smooth surfaces. Specifically, we apply our theoretical results to structural transitions within dense monolayers formed by alkanes on graphite. The latter have been studied recently by scanning tunneling microscopy (STM) of the interface between organic solutions containing long chain alkanes and the basal plane of graphite. Over a wide range of solute concentrations, the STM images show highly ordered monolayers consisting of solute molecules in all-trans conformation densely physisorbed parallel to the surface.^{8,9,10} The observed ordering within the monolayer depends on both temperature and molecular weight,¹¹ i.e., the alkane chain length, and, in addition for bidisperse solutes, on the adsorbate composition (see also Ref. 12). The monolayer structure may vary between highly ordered crystalline lamellae and less ordered columnar structures. Even though our theory neglects the details of the intra-adsorbate and adsorbate-substrate interactions, we obtain a close correspondence between the high density region in the model phase diagram and the experimental observations, which illuminates the nature of the different types of ordering observed in the alkane monolayers.

THE MODEL

The method used here is an application of a recent excluded volume model for lyotropic liquid crystalline behavior of monodisperse orientationally ordered hard rigid spherocylinders in three dimensions.⁶ The description of the various possible translationally ordered phases is based on the trade-off of translational entropy between translationally disordered liquidlike dimensions and translationally ordered crystal-like dimensions. Within this model the dimensionless configurational free energy per particle is approximated in each phase as $f_d^{\text{conf}} = \ln \rho - 1 + f_d^{\text{fluid}} + f_{3-d}^{\text{cryst}}$, where ρ is the particle number density and f_d^{fluid} is the nonideality contribution from d fluidlike dimensions,

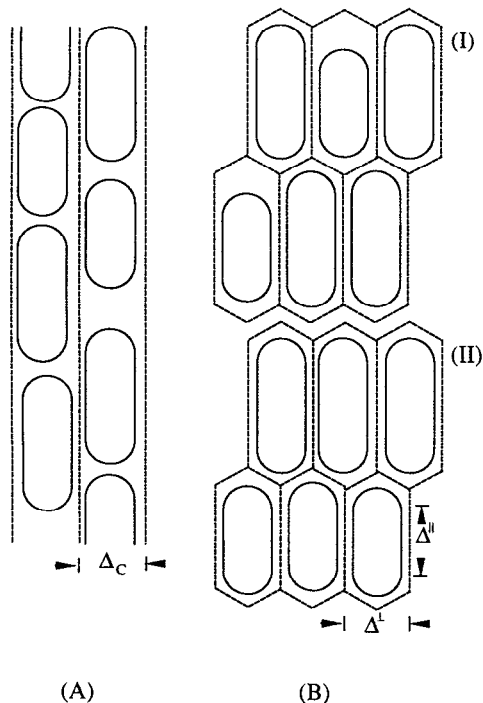


FIG. 1. (a) Illustration of model particles of length $L_1 + D$ and $L_2 + D$ confined to columnar channels of width Δ_c . (b) Schematic of two different types of crystalline order. (I) shows all particles confined to identical hexagonally packed cells irrespective of their length. (II) shows each type of particle confined within its specific type of cell.

whereas f_{3-d}^{cryst} is the nonideality contribution from the remaining $(3-d)$ crystal-like dimensions. Within this scheme $d=3$ for a nematic fluid, $d=2$ for a smectic phase (i.e., two fluid dimensions and one crystalline dimension), $d=1$ for a columnar phase (i.e., one fluid dimensions and two crystalline dimensions), and $d=0$ for a crystalline phase (i.e., three crystalline dimensions). Good approximations for the nonideality contributions to f_d^{conf} can be obtained by using the scaled particle approach¹³ for f_d^{fluid} , whereas for f_{3-d}^{cryst} simple one particle cell models are quite adequate.⁷

In the following, we consider the analogous bidisperse two-dimensional system, where the spherocylinders are constrained to move along a planar interface. Similarly to the three-dimensional system, we consider ordering of parallel rectangles of length L_i capped by hemicycles of diameter D into nematic, columnar, and crystalline order (smectic ordering is omitted for reasons explained below). The nematic phase is simply a two-dimensional fluid of oriented particles. In the model columnar phase the particles retain fluidlike behavior only in the direction of their long axis, whereas in the orthogonal direction they are confined between hard walls. The picture is that of a one-dimensional fluid of rods within a hard channel corresponding to a one-dimensional cell [as illustrated in Fig. 1(a)]. Notice that the dimensional separation of f_d^{conf} is a good approximation only if the channels are narrow enough to prohibit the side-by-side doubling up of rods. Because the width of the columnar channel is not an ad-

justable parameter, it additionally provides a consistency check on the model. We return to this point below. Finally, in the crystalline phase each particle is confined within an impenetrable hard cell [cf. Fig. 1(b)]. Under these assumptions the configurational free energy of the binary mixture can approximately be written as

$$f_d^{\text{conf}} = \ln \rho - (1 - \delta_{0d}) + \sum_{i=1}^2 y_i \ln y_i + f_d^{\text{fluid}} + f_{2-d}^{\text{crystal}}, \quad (1)$$

where y_i denotes the fraction of particles of length L_i . The first three terms are the contribution of noninteracting point particles of type $i=1,2$, where the δ -function accounts for the distinguishability of the particles in the crystalline phase. As before, f_d^{fluid} is the excluded volume contribution to the free energy of a d -dimensional fluid, and f_{2-d}^{crystal} is the free energy contribution accounting for the reduction of the available cell volume within a $(2-d)$ -dimensional crystal due to the finite size of the particles.

For the nematic phase ($d=2$), f_2^{fluid} can be quite accurately described using scaled particle theory (cf. e.g., Ref. 14) which yields

$$f_2^{\text{fluid}} = -\ln(1-v) + \frac{v}{1-v}, \quad (2)$$

where v is the particle volume fraction. Note that due to the orientational constraint on our model particles, Eq. (2) coincides with the result for hard disks.¹⁵ Notice also that $f_0^{\text{crystal}} = 0$ in this case. The nematic equation of state thus becomes

$$p_2 = \frac{\rho}{(1-v)^2}, \quad (3)$$

where p_2 is the nematic pressure divided by $k_B T$.

In the columnar case ($d=1$), f_1^{fluid} can again be obtained via scaled particle theory, which yields the exact result (cf. Ref. 15)

$$f_1^{\text{fluid}} = -\ln(1-v_1), \quad (4)$$

where v_1 is the one-dimensional volume fraction along the columnar tube. Here v_1 is simply given by $v_1 = (\bar{L} + D)\Delta_c \rho$, where $\bar{L} + D = \sum_{i=1}^2 y_i L_i + D$ is the mean length of the particles and Δ_c is the width of the columnar channel. Analogous to the previous results for three dimensions,⁷ f_1^{crystal} is given by the negative logarithm of the ratio of the free volume to the cell volume, i.e.,

$$f_1^{\text{crystal}} = -\ln\left(\frac{\Delta_c - D}{\Delta_c}\right). \quad (5)$$

Note that Δ_c follows from the condition $\partial f^{\text{conf}} / \partial \Delta_c = 0$, which yields

$$\Delta_c = \sqrt{\frac{D}{(\bar{L} + D)\rho}}. \quad (6)$$

Using Eqs. (4)–(6), we obtain for the columnar pressure

$$p_1 = \frac{\rho}{1 - \sqrt{D(\bar{L} + D)\rho}}. \quad (7)$$

In the special case $L_i=0$, i.e., when the particles are hard disks, the crystalline order at high densities is hexagonal, and thus the corresponding cells containing the particles will form a honeycomb lattice. The natural extension for monodisperse rodlike particles, i.e., $L_1=L_2>0$, is a lattice of stretched honeycombs [cf. Fig. 1(b)]. The bidisperse case, however, is more complicated and we consider two plausible alternatives, i.e., (I) long and short particles are mixed and all cells are identical or (II) the particles separate according to their length and there are two corresponding types of cells [cf. Fig. 1(b)]. The explicit calculation shows that within our model, structure (I) is always less stable than structure (II). Thus, because the respective calculations are completely analogous, in the following we only discuss structure (II). In this case, the configurational cell free energy (cf. Ref. 16) can be written as

$$f_0^{\text{conf}} = - \sum_{i=1}^2 y_i \ln \alpha_i^{\text{free}}, \quad (8)$$

where the free volume α_i^{free} for a particle of type i is given by

$$\alpha_i^{\text{free}} = \frac{\sqrt{3}}{2} (\Delta_i^\perp - D)^2 + (\Delta_i^\parallel - L_i)(\Delta_i^\perp - D). \quad (9)$$

Note that Δ_i^\perp and $(2/\sqrt{3})\Delta_i^\perp + \Delta_i^\parallel$ are the diameter and the length of a crystal cell of type i , respectively [cf. Fig. 1(b)]. Analogous to the columnar case, the crystalline Δ 's follow from $\delta_\Delta(f_0^{\text{conf}} + \lambda/\rho) = 0$, the variation of f_0^{conf} with respect to the cell dimensions Δ_i^\perp and Δ_i^\parallel . Here λ is a Lagrange multiplier conjugate to the condition that $\sum_{i=1}^2 y_i \alpha_i^{\text{free}} = V/N = 1/\rho$ is constant, where α_i denotes the volume of a cell occupied by a particle of type i , V is the total volume, and N is the number of particles. The above variation yields

$$\frac{y_2 b_1}{y_1 b_2} \left[\left(\frac{\Delta_1^\perp}{D} \right)^2 - \frac{\Delta_1^\perp}{D} \right] + \sqrt{\frac{1}{b_2 \rho D^2} - \frac{b_1}{b_2} \left(\frac{\Delta_1^\perp}{D} \right)^2} \times \left[1 - \sqrt{\frac{1}{b_2 \rho D^2} - \frac{b_1}{b_2} \left(\frac{\Delta_1^\perp}{D} \right)^2} \right] = 0, \quad (10)$$

where $b_i = y_i(\sqrt{3}/2 + L_i/D)$, from which Δ_1^\perp can be calculated numerically. The other Δ 's follow subsequently from the additional equations

$$\sum_{i=1}^2 b_i \Delta_i^{\perp 2} = \rho^{-1} \quad (11)$$

and

$$\Delta_i^\parallel = (L_i/D) \Delta_i^\perp. \quad (12)$$

Using Eqs. (8)–(12) the crystalline pressure becomes

$$p_0 = -\rho \sum_{i=1}^2 y_i \frac{1}{\alpha_i^{\text{free}}} \left[(\Delta_i^\perp - D) \frac{L_i}{D} + [\sqrt{3}(\Delta_i^\perp - D) + (\Delta_i^\parallel - L_i)] \right] \frac{\partial \Delta_i^\perp}{\partial \rho}, \quad (13)$$

where the derivatives are given by

$$\frac{\partial \Delta_1^\perp}{\partial \rho} = - \left[2\rho^2 b_1 \Delta_1^\perp \left(1 + \frac{y_2 \Delta_2^\perp 2\Delta_1^\perp - D}{y_1 \Delta_1^\perp 2\Delta_2^\perp - D} \right) \right]^{-1} \quad (14)$$

and

$$\frac{\partial \Delta_2^\perp}{\partial \rho} = \frac{y_2 b_1 (2\Delta_1^\perp - D)}{y_1 b_2 (2\Delta_2^\perp - D)} \frac{\partial \Delta_1^\perp}{\partial \rho}. \quad (15)$$

Whereas the monodisperse f_d^{conf} is immediately obvious for the nematic and columnar cases, the explicit equation in the crystalline case is given below. Using Eqs. (11) and (12), we obtain $\Delta^\perp = [(\sqrt{3}/2 + L/D)\rho]^{-1} = D\sqrt{v_{\text{cp}}/v}$ and $\Delta^\parallel = L\sqrt{v_{\text{cp}}/v}$, where v_{cp} denotes the volume fraction at close packing. Inserting this into Eq. (9) and the result into Eq. (8) yields the monodisperse f_0^{conf} in the form of Eq. (1), where now

$$f_0^{\text{crystal}} = -2 \ln(1 - \sqrt{v/v_{\text{cp}}}). \quad (16)$$

This is identical to the well known result for hard disks¹⁷ and analogous to the three dimensional result for parallel spherocylinders.⁷ Additionally, using Eq. (16), the pressure becomes

$$p_0 = \frac{\rho}{1 - \sqrt{v/v_{\text{cp}}}}. \quad (17)$$

So far, we have used the intuitive self-consistent free volume (SCFV) model,¹⁸ characterized by space filling non overlapping cells, to describe the free volume for crystalline order in one and two dimensions. However, it is known from studies on hard disks and hard spheres that this model severely underestimates the free volume.¹⁹ This shortcoming can largely be overcome by a simple but somewhat ad hoc extension. Concretely, this means that the volume available to a particle is uniformly increased (conserving the shape of the cell) until it starts to overlap with the neighboring particles located at the center of their cells. It is easy to see that the resulting Lennard-Jones–Devonshire (LJD) cell free energies can be obtained from our above self-consistent free volume energies by the simple relation

$$f_d^{\text{conf(LJD)}} = f_d^{\text{conf(SCFV)}} - (2-d) \ln 2, \quad (18)$$

i.e., all this amounts to is the scaling of the free volume by a factor 2 in the columnar case and a factor 4 in the crystalline case.

We can now compare the different LJD-free energies to determine the stable phase corresponding to the lowest free energy for a given set of the parameters v , y_i , and L_i/D . Phase diagrams are calculated in the usual fashion equating the pressures p_d and the chemical potentials $\mu_d = f_d + p_d/\rho$.

PHASE DIAGRAM FOR MONODISPERSE RODS AND ITS RELATION TO STM STUDIES ON ALKANES PHYSORBED ON GRAPHITE

Figure 2(a) shows the phase diagram for the monodisperse system (i.e., $L_1=L_2=L$) in terms of the reduced particle volume fraction v/v_{cp} and the rod length L/D . For short rods, i.e., $L/D \lesssim 2$ we obtain a direct transition from

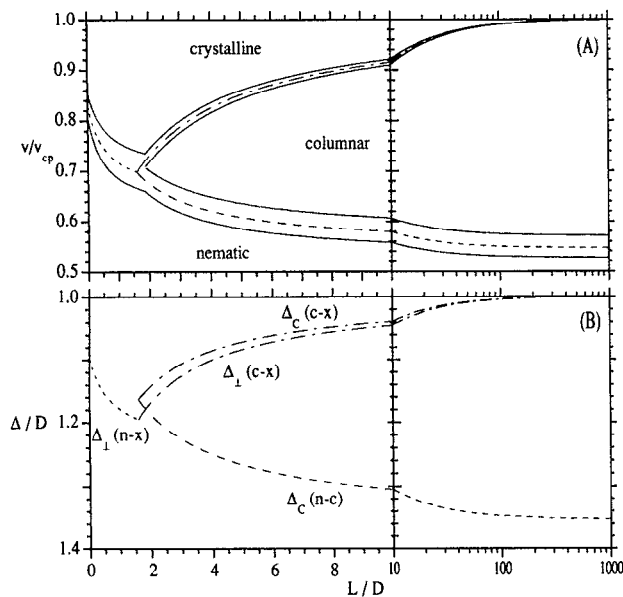


FIG. 2. (a) Theoretical phase diagram for monodisperse model particles in terms of aspect ratio L/D and reduced volume fraction v/v_{cp} , where v is the two-dimensional volume fraction and v_{cp} is the corresponding close packing volume fraction given by $v_{cp} = (\pi^2/(8\sqrt{3}) + L/D)/(\pi/4 + L/D)$. Solid lines indicate phase coexistence. Dashed lines indicate the intersection of the respective free energies. (b) Widths of the columnar and crystalline cells (cf. Fig. 1) at the free energy crossings of (a). Note that $(n-c)$ indicates the cross over from nematic to columnar, $(n-x)$ indicates the cross over from nematic to crystalline, and $(c-x)$ indicates the cross over from columnar to crystalline.

the nematic to the crystalline phase with increasing volume fraction. It is worth noting that at $L/D=0$ the boundaries of the coexistence region are located at $v_{nem}=0.734$ and $v_{cryst}=0.776$, which is reasonably close to the classical molecular dynamics simulation result of Alder and Wainwright for the freezing transition in the hard disk fluid,²⁰ i.e., $v_{liquid}=0.69$ and $v_{solid}=0.72$. For $L/D \gtrsim 2$, the columnar phase intervenes between the nematic and the crystalline phase, and as L/D increases, the density range over which the columnar phase is stable widens. In the limit $L/D \rightarrow \infty$, it is easy to see from Eqs. (2), (4), (5), (6), and (18) that the free energy cross over from nematic to columnar order is determined by the relation $\ln[2(1-\sqrt{v})^2/(1-v)] + v/(1-v) = 0$, which yields $v_{n-to-c} = 0.546$ (Note that $v_{cp} = 1$ for $L/D = \infty$). The cross over from columnar to crystalline order, on the other hand, asymptotically approaches 1. Figure 2(b) shows the values of Δ_c and Δ_l along the cross over volume fractions indicated by the dashed lines in Fig. 2(a). It is worth noting that both the width of the columnar tube Δ_c as well as the width of the crystal cell Δ_l are always sufficiently narrow (in the range of volume fractions over which the respective phases are stable) to prevent the doubling up of the rods (cf. below). Notice also that, at the columnar to crystalline cross over, the columnar channels are slightly narrower than the corresponding crystalline cells.

In the following, we want to draw the correspondence between the theoretical results and recent STM studies at

the interface between organic solutions of long chain alkanes and the basal plane of graphite. It is well known for such systems that, over a wide range of solute concentrations, the alkanes form dense monolayers on the graphite surface.²¹ STM studies of the monolayers reveal that the alkanes are adsorbed in all-trans conformation parallel to the graphite surface.^{8,9} This is illustrated in Fig. 3, which displays a series of STM images showing alkane monolayers, prepared at the interface between solutions of the alkanes in 1-phenyloctane and the graphite basal plane at room temperature, as described before.⁹ The molecular weight of the monodisperse alkane chains increases from $C_{24}H_{50}$ in Fig. 3(a) to $C_{192}H_{386}$ in Fig. 3(c). The shorter alkanes in the Figs. 3(a) and 3(b) exhibit highly ordered lamellar structures corresponding to crystalline order, whereas for the particularly long alkane in Fig. 3(c) no lamellae have been observed. However, even for the long alkane there remains a pronounced one-dimensional contrast modulation consistent with a dense side-by-side packing of the alkane chains.²² It should be noted in this context that $C_{50}H_{102}$ may be a borderline case, since for this material orientationally ordered nonlamellar structures have been found also.¹⁰ In order to compare the STM results to our theoretical phase diagrams it is necessary to know the density in the alkane monolayers, which is determined by the chemical potential difference between the solution and the adsorbate layer. The STM images of the highly ordered monolayers calibrated against the substrate lattice indicate packing densities very similar to the bulk material,⁹ i.e., certainly within 10% of close packing. Less dense monolayers seem to be too mobile to be imaged by STM. Thus we can interpret the sequence of STM images in Fig. 3 in terms of a constant volume fraction cut through the phase diagrams in Fig. 2(a) at high packing densities. In order to relate the model parameters D and L to real alkane chains, we have performed energy minimizations on $C_{24}H_{50}$ dimers based on the atomic AMBER force field (using the same parameters as in Ref. 23). For a side-by-side configuration of all-trans chains with their zig-zag planes parallel, we obtain ~ 4.2 Å for the optimized separation of the chain axes, whereas for a linear arrangement the optimized distance of equivalent atoms in the two molecules is ~ 33 Å. Thus we set $D=4.2$ Å and $L+D=33$ Å and therefore $L/D=6.9$ Å. Estimates for different alkane chains can be obtained according to $(L/D)_{C_nH_{2n+2}} \approx n/m(L/D)_{C_mH_{2m+2}}$.

In both the theoretical phase diagrams as well as in the sequence of STM images displayed in Fig. 3 we find crystalline order for short particles. For increasing particle length, however, the theoretical phase diagram eventually predicts a transition from the crystalline phase into a columnar phase. Indeed, the concept of the columnar phase with one-dimensional crystalline order perpendicular to the particles long axes and fluid behavior along the channel, is consistent with the STM image of $C_{192}H_{386}$ [Fig. 3(c)]. Here the STM contrast modulation perpendicular to the main axis of the alkanes corresponds to the one-dimensional crystalline order, whereas the absence of any discernable contrast modulation along the alkane chain di-

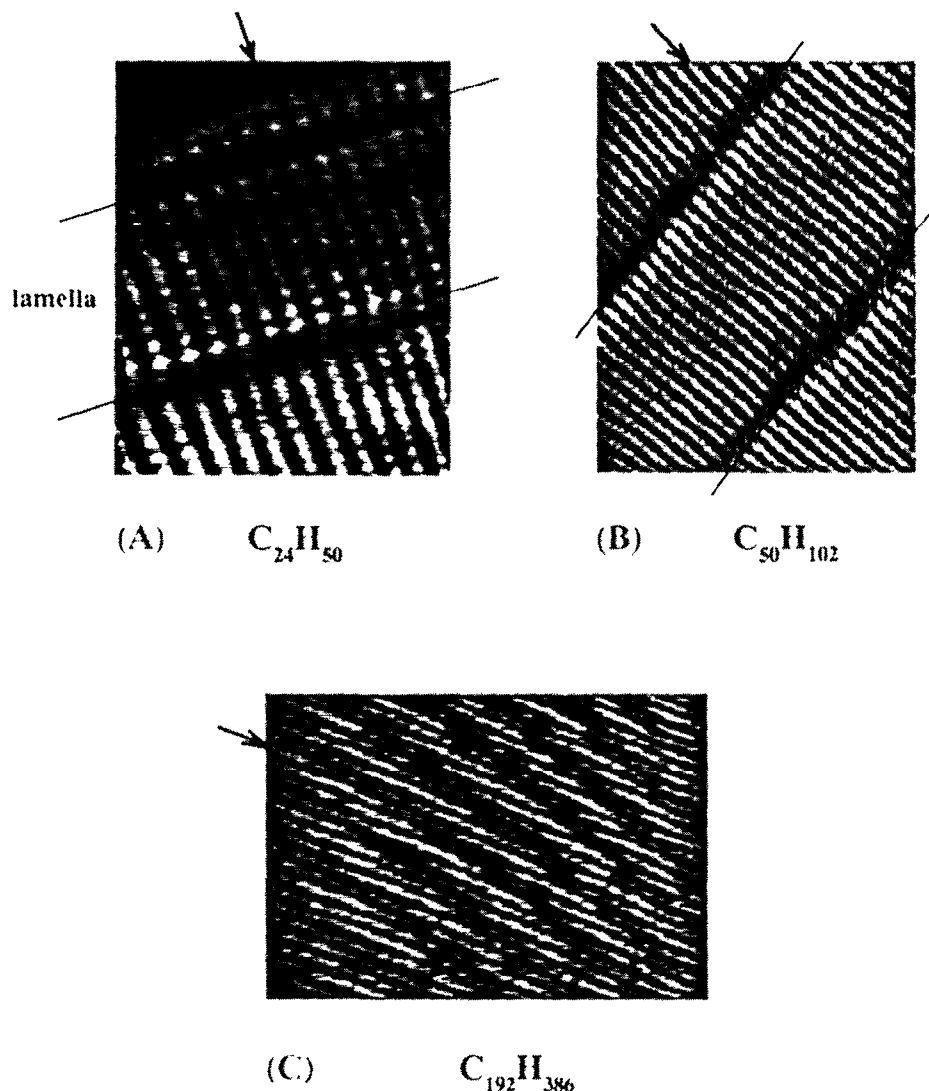


FIG. 3. STM images of monolayers of monodisperse alkanes at the interface between the basal plane of graphite and a solution of long chain alkanes in 1-phenyloctane. (a) and (b) show crystalline lamellae of $C_{24}H_{50}$ (Ref. 23) and $C_{50}H_{102}$ (Ref. 10), where the orientation of the molecules (indicated by the arrows) is perpendicular to the lamella boundaries (indicated by straight lines). (c) shows a STM image of $C_{192}H_{386}$ (Ref. 11) lacking a lamellar structure. However, a contrast modulation (perpendicular to the molecular orientation indicated by the arrow) consistent with dense side-by-side packing of the alkane chains is clearly discernible (see also Ref. 22).

rection can be interpreted in terms of the increased mobility of the molecules along this direction.

PHASE DIAGRAMS FOR BIDISPERSE ROD MIXTURES AND COMPARISON TO RELATED STM RESULTS ON ALKANES PHYSORBED ON GRAPHITE

Figure 4 shows a series of theoretical phase diagrams for selected values of L_1/D and L_2/D in terms of reduced volume fraction v/v_{cp} and the fraction of longer rods. The first two rows correspond to mixtures of slightly elongated particles $L_1/D > 0$ with disks $L_2/D = 0$. The two values for L_1/D correspond to particle lengths below and above the triple point in Fig. 2(a). Notice that for mixtures with $L_1/D = 1.5$ and $L_2/D = 0$ columnar ordering may be stable over a range of mixing ratios, even though the respective

monodisperse systems do not show stable columnar ordering. For mixtures with $L_1/D = 4.0$ and $L_2/D = 0$ the behavior is expected, i.e., for small fractions of elongated particles there is a direct nematic-to-crystalline transition, whereas finally the columnar phase intervenes. Interesting, however, is the possibility of a crystalline-to-columnar-to-crystalline re-entrant transition for constant v/v_{cp} , which we address in more detail below. For mixtures of longer particles, i.e., both L_1/D and L_2/D are to the left of the triple point in Fig. 2(a), as exemplified in the last three rows, there is always a columnar phase independent of the mixing ratio. In addition, the range of volume fractions over which the columnar phase is stable progressively widens with increasing particle lengths. As a function of the fraction of long rods, the nematic-to-columnar transition shifts monotonously between the transition volume frac-

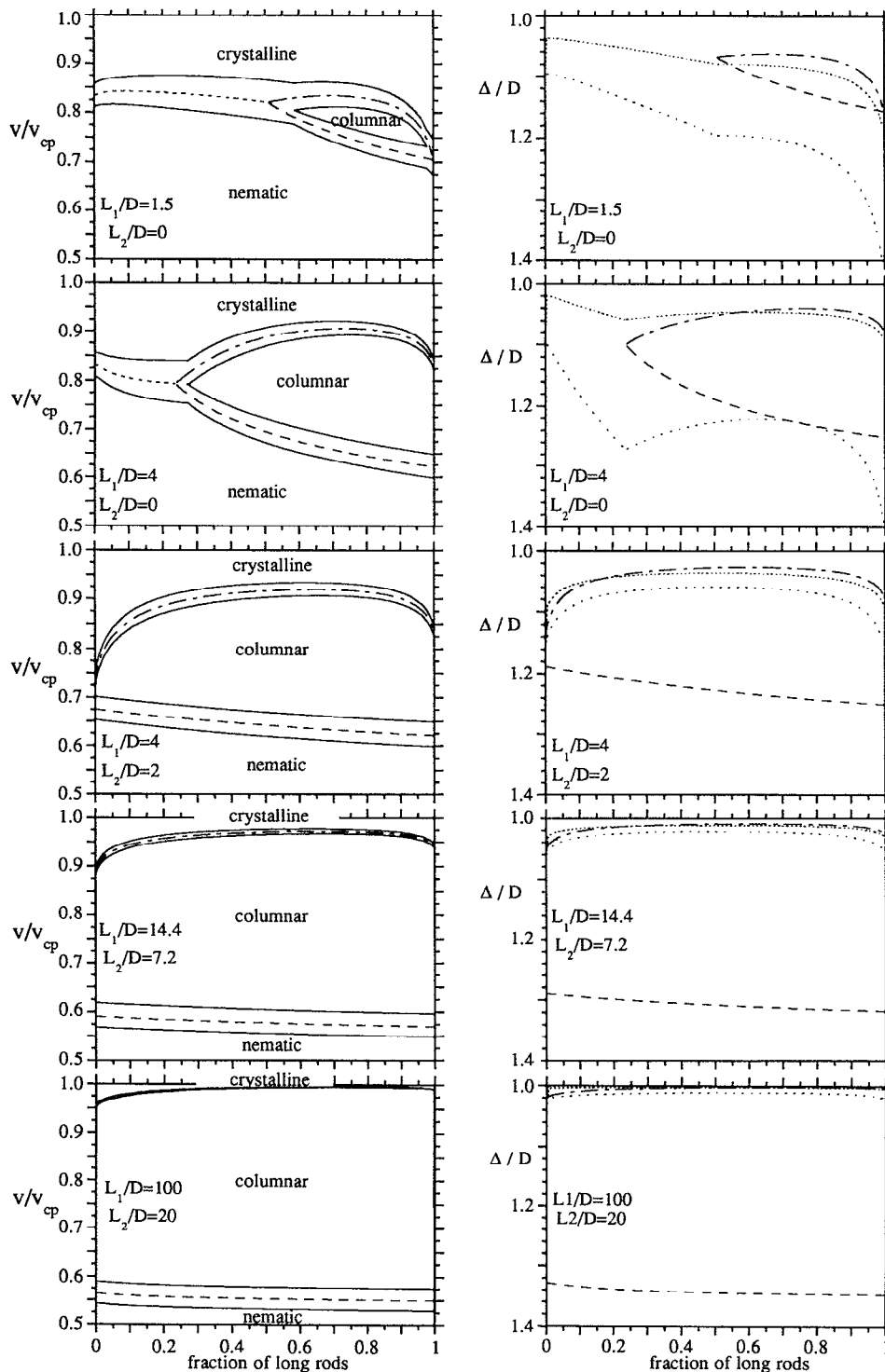


FIG. 4. Phase diagrams of the bidisperse mixture in terms of the fraction of longer rods and the reduced volume fraction v/v_{cp} (left) and corresponding cross over cell widths in terms of the fraction of longer rods (right) for different combinations of L_1/D and L_2/D (indicated in the panels). Note that here $v_{cp} = \sum_{i=1}^2 \nu_i \nu_{cp,i}$ where $\nu_{cp,i} = [\pi^2/(8\sqrt{3}) + L_i/D]/(\pi/4 + L_i/D)$. In the phase diagrams, solid lines indicate phase coexistence, short dashes indicate nematic-to-crystalline cross over, long dashes indicate the nematic-to-columnar cross over, and long-short dashes indicate the columnar-to-crystalline cross over. In the panels for the cell widths, long dashed lines show Δ_c at the nematic-to-columnar cross over, long-short dashed lines show Δ_c at the columnar-to-crystalline cross over, closely spaced dots indicate Δ_1^c , i.e., the crystalline cell width for the longer particles, at the cross over to crystalline stability, and widely spaced dots indicate Δ_2^c , i.e., the crystalline cell width for the shorter particles, at the cross over to crystalline stability.

tions of the corresponding pure systems composed of only short or only long particles. For the columnar-to-crystalline transition, however, there is again a range of volume fractions where we encounter a crystalline-to-columnar-to-crystalline phase sequence as a function of composition. Analogous to Fig. 2(b), the right panels in Fig. 4 show the various cell widths at the free energy cross overs indicated as dashed lines in the corresponding phase diagrams. Notice that always $\Delta_1^\perp < \Delta_2^\perp$, i.e., the longer particles occupy the narrower cells. However, this effect is only significant for the rather short particles in the first two panels. Notice also that this induces a mismatch of the cells along domain boundaries between long and short lamellae [cf. Fig. 1(b)], which is not explicitly included in the present theory, but should disfavor this type of domain boundary due to the attendant unfavorable packing.

Analogous to the monodisperse case, it is possible to prepare alkane monolayers composed of alkanes with different molecular weight. However, the lack of control of the surface density (see above) is now compounded by the lack of control on the mixing ratio within the monolayer, which is generally not identical to the solute concentration ratio in the bulk solution. Thus, our comparison with the experimental observations is again qualitative in nature. Figure 5 displays a series of three STM images of mixed alkane monolayers containing $C_{25}H_{52}$ and $C_{50}H_{102}$, adsorbed from concentrated but not saturated solutions in 1-phenyloctane at a total concentration of 7 mg/ml and a molar ratio between long and short molecules of $\sim 10^{-4}$. Figures 5(a) and 5(c) exhibit a crystalline phase of predominantly $C_{25}H_{52}$ and $C_{50}H_{102}$, respectively, with short lamellae of probably 3 and 7 molecules, respectively, of the other component. The images correspond to the edges of the phase diagram for $L_1/D=14.4$ and $L_2/D=7.2$ displayed in Fig. 4. At an intermediate mixing ratio, Fig. 5(b) shows a columnar phase in the sense explained above, i.e., the molecules retain their orientation parallel to a graphite lattice axis as well their side-to-side distance commensurate with the substrate, but they lose the lamellar order. They also exhibit a considerable mobility along the columns, which makes it impossible to observe molecular ends on the STM-time scale, i.e., on the order of milliseconds.²⁴ Note that the sequence of STM images in Fig. 5 is consistent with a cut at $v/v_{cp} \sim 0.95-0.97$ through the theoretical phase diagram for $L_1/D=14.4$ and $L_2/D=7.2$ in Fig. 4. Columnar phases, which are indistinguishable from Fig. 5(b) have also been readily obtained for other bidisperse alkane monolayers including $C_{20}H_{42}/C_{24}H_{50}$ and $C_{24}H_{50}/C_{32}H_{66}$ over a large concentration range. Mixed crystalline phases have been observed before in a long chain alkanol monolayer.¹² For alkanes they are relatively difficult to obtain. The system chosen here is special in the sense that two short lamellae may replace rather well one long lamella without causing much stress in the monolayer. An even better match is the system $C_{24}H_{50}/C_{50}H_{102}$, in which we have only observed crystalline and no columnar ordering, indicating a higher monolayer density (cf. Fig. 4). It should be noted that the considerable difference in molecular weight implies a strong tendency for prefer-

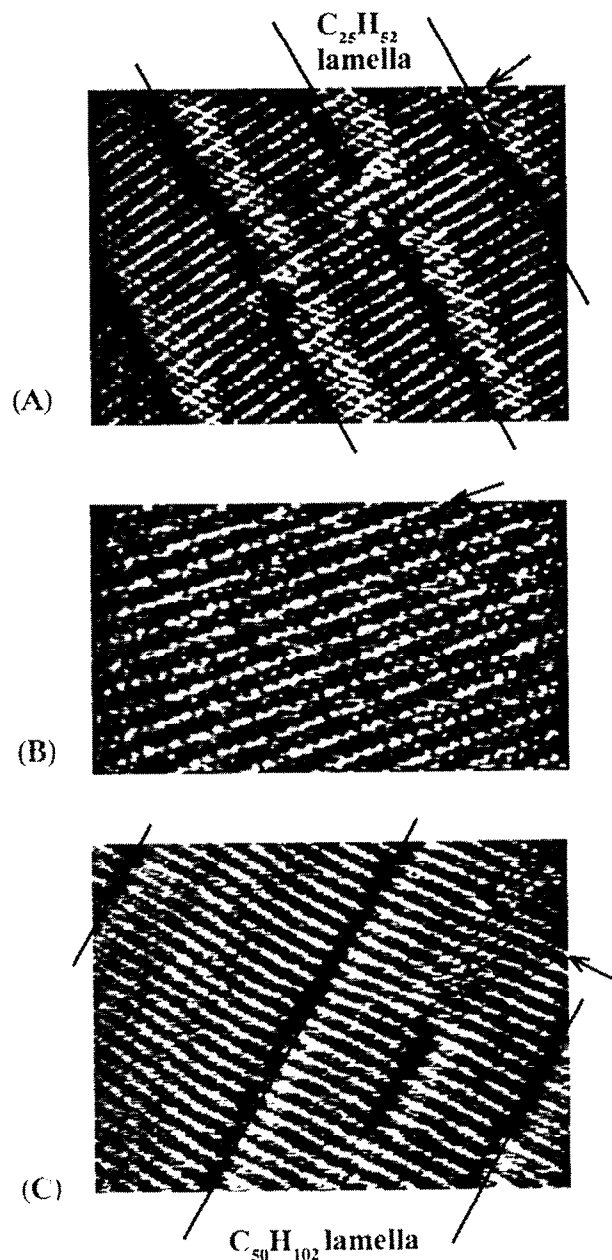


FIG. 5. STM images of a bidisperse alkane monolayer of $C_{25}H_{52}$ and $C_{50}H_{102}$ adsorbed at the interface between the basal plane of graphite and an organic solution. (a) and (c) show crystalline phases of predominantly short and long rods, respectively, with small crystallites of the other component incorporated. In the center of (a), there are three neighboring $C_{50}H_{102}$ molecules (located in the break of the line indicating the middle lamellar boundary) across the width of two $C_{25}H_{52}$ lamellae. In the lower right of (c), there are seven neighboring pairs of $C_{25}H_{52}$ molecules within a $C_{50}H_{102}$ lamella. (b), on the other hand, shows a columnar phase. Using the graphite lattice, underlying the image, as an internal Ref. 9, we find that the columns of molecular rods are oriented parallel to a graphite lattice axis with a regular spacing between the columns, which is commensurate with the graphite lattice and equal to the intermolecular spacing in the crystalline alkane lamellae. The mobility along the columns is too high to allow the observation of the ends of the molecules.

ential adsorption of the longer component, which means that one has to use the shorter component in large excess in the bulk solution, in order to avoid the formation of crystals of the longer component only. Furthermore, due to the

finite exchange with the ambient, the molar ratio in the adsorbed layer may vary slightly across the surface as well as in time, which means that crystalline and columnar phases may be found simultaneously on a particular surface. In fact, all three images displayed in Fig. 5 have been obtained at the same macroscopic conditions.

DISCUSSION

Based on an intuitive model for various types of translational order for parallel rodlike particles in two dimensions, we have obtained phase diagrams, which can successfully predict structural transitions observed in STM studies on long chain alkanes physisorbed on graphite. In obtaining these results, we have made a number of assumptions. For the case of three dimensions the model assumptions are discussed in detail in Refs. 6 and 7, and most of the reasoning there also applies in the present case. One major difference that deserves extra mentioning is that in the three dimensional monodisperse system stable smectic order intervenes between the nematic and columnar phases for long rods. However, the two-dimensional analog of the three-dimensional model for smectic order is basically identical to the above model for columnar order, where now the fluid dimension is perpendicular to the long axis of the particles, and the columnar "channel" is replaced by the smectic "row." Whereas this type of order is clearly unfavorable in the bidisperse case, in the monodisperse case, our model actually cannot distinguish it from the columnar order discussed above.

In comparing our theoretical results to the experiments, we assume first of all that the alkanes on the flat surface behave as rods rather than coiling up like in the bulk solution. This seems justified on the basis of adsorption isotherm measurements²¹ and our STM images. Moreover, we assume that the inter alkane interactions are well approximated in terms of hard core repulsions. This seems reasonable because at the high concentrations considered here, the alkane interaction is determined mainly by steric repulsion. Furthermore, there is no significant charge polarization giving rise to long range Coulomb interactions. In cases where they are important, the latter might be included in the model via an effective particle shape and/or particle size, or they might also render the present approach inapplicable. Regarding the adsorbate substrate interaction, it is well known that generally the corrugation of the substrate plays a role in the formation of a particular adsorbate layer. In the model, however, we neglect all details of the adsorbate surface interaction and treat the surface as ideally smooth. This is motivated by the idea that for large physisorbed chain molecules at finite temperatures the influence of the substrate corrugation is reduced due to the usually occurring incommensurability between the adsorbate molecules' repeat unit and the substrate lattice periodicity, and, in addition, due to the thermally excited backbone fluctuations of the chain even at dense packing (cf. Ref. 23). Nevertheless, the STM observations show in most cases a preferential orientation of the alkane chains along the carbon rows of the graphite lattice, indi-

cating an ordering effect due to the graphite substrate which would tend to favor columnar ordering as defined in the model.

An aspect neglected thus far is molecular flexibility, which should become important for strongly elongated particles. For the sake of concreteness, we assume that elongated particles are continuous bend-elastic, i.e., persistent flexible, which is reasonable for alkane chains forming dense monolayers. In this case, the loss of entropy due to the constraints on the particles contour undulations in the plane imposed by the presence of their lateral neighbors, gives rise to an additional contribution to the free energy. This confinement free energy favors the phase which provides maximum lateral freedom. At constant volume fraction, obviously nematic order is less favorable than columnar order according to this criteria. After all, it is the trade-off between positional entropy and packing efficiency, which drives the transition. Similarly, crystalline order is favored over columnar order. This can, for instance, be seen for the monodisperse case in Fig. 2(b), where indeed $\Delta_c < \Delta^1$. Thus, we expect that the main effect of including flexibility is to shift the transitions discussed here to somewhat lower densities.²⁵

Finally, as already mentioned above, the imposition of the stringent positional constraints forces all transitions to be discontinuous and tends to increase the transition densities due to the exaggeration of order near the transition. In this context it is of speculative interest to apply an argument by Sluckin,²⁶ who calculates the transition volume fraction and the transition layer spacing in the case of the nematic to smectic-A transition for hard parallel rods in three dimensions, which is believed to be second order, to the nematic to columnar transition in two dimensions. Assuming a continuous transition, the location of the transition is determined by the divergence of the structure factor $S(\mathbf{k}) = [1 - \rho c(\mathbf{k})]^{-1}$, where the direct correlation function is $c(\mathbf{r}) \approx -(1-v)^{-1}$ if the two particles overlap and $c(\mathbf{r}) = 0$ otherwise. In the limit for long rods, $v \approx DL\rho$ and $c(\mathbf{k}) \approx -2L(1-v)^{-1} \int_{-D}^D \exp(ikz) dz = -4v(1-v)^{-1} (kD)^{-1} \sin(kD)$, where z denotes the direction perpendicular to the columnar axis. Note that $c(\mathbf{k})$ attains its maximum for $k_c D = 4.493$, and thus $S(\mathbf{k})$ diverges at $v_{n-to-c} = 0.535$, where the wave length of the columnar density fluctuations in units of D is $2\pi/(k_c D) = 1.398$. The quantities corresponding to v_{n-to-c} and $2\pi/(k_c D)$ in our model are the volume fraction and the width of the columnar channels at the free energy cross over from nematic to columnar order. As shown above, our model yields $v_{n-to-c} = 0.546$ and $\Delta_c/D = 1.353$, which is interestingly close.

In conclusion, even though the present model employs a number of crude approximations, it is intuitive and it yields a series of results, which are useful for the understanding of the nature of the structural transitions observed by STM in dense monolayers of long chain alkanes. In particular, it predicts transitions between crystalline and columnar phases in bidisperse systems, which could also be observed experimentally.

ACKNOWLEDGMENTS

We are grateful to C. Kröhnke and G. Wenz for the donation of $C_{192}H_{386}$.

- ¹L. Onsager, *Ann. N.Y. Acad. Sci.* **51**, 627 (1949).
- ²D. Frenkel, in *Liquids, Freezing and Glass Transition*, Les Houches 1989, Session LI (Part II) (North-Holland, Amsterdam, 1991).
- ³T. Odijk, *Macromolecules* **19**, 2313 (1986).
- ⁴A. N. Semenov and A. R. Kokhlov, *Sov. Phys. Usp.* **31**, 988 (1988).
- ⁵A. Y. Grossberg and A. R. Kokhlov, *Soc. Sci. Rev. A Phys.* **8**, 147 (1987).
- ⁶M. P. Taylor, R. Hentschke, and J. Herzfeld, *Phys. Rev. Lett.* **62**, 800 (1989).
- ⁷R. Hentschke, M. P. Taylor, and J. Herzfeld, *Phys. Rev. A* **40**, 1678 (1989).
- ⁸G. C. McGonigal, R. Bernhardt, and D. J. Thomson, *Appl. Phys. Lett.* **57**, 28 (1990).
- ⁹J. P. Rabe and S. Buchholz, *Science* **253**, 424 (1991).
- ¹⁰J. P. Rabe and S. Buchholz, *Makromol. Chem. Macromol. Symp.* **50**, 261 (1991).
- ¹¹L. Askadskaya and J. P. Rabe, *Phys. Rev. Lett.* **69**, 1395 (1992).
- ¹²S. Buchholz and J. P. Rabe, *Angew. Chem. Int. Ed. Engl.* **31**, 189 (1992).
- ¹³H. Reiss, H. L. Frisch, and J. L. Lebowitz, *J. Chem. Phys.* **31**, 369 (1959).
- ¹⁴M. A. Cotter and D. C. Wacker, *Phys. Rev.* **18**, 2669 (1978).
- ¹⁵E. Helfand, H. L. Frisch, and J. Lebowitz, *J. Chem. Phys.* **34**, 1037 (1961).
- ¹⁶T. L. Hill, *An Introduction to Statistical Thermodynamics* (Dover, New York, 1986).
- ¹⁷L. Tonks, *Phys. Rev.* **50**, 955 (1936).
- ¹⁸W. W. Wood, *J. Chem. Phys.* **20**, 1334 (1952).
- ¹⁹B. J. Alder, W. G. Hoover, and D. A. Young, *J. Chem. Phys.* **49**, 3688 (1968).
- ²⁰B. J. Alder and T. E. Wainwright, *Phys. Rev.* **127**, 359 (1962).
- ²¹G. H. Findenegg and M. Liphard, *Carbon* **25**, 119 (1987).
- ²²Figure 3(d) actually shows two superimposed contrast modulations. The short period is consistent with a side-by-side packing of the alkanes. The long period can be attributed to a moirée pattern between substrate and adsorbate lattice, indicating that the alkane chains, rather than being aligned along the substrate carbon rows, are rotated by $\sim 15^\circ$ with respect to the substrate lattice.
- ²³R. Hentschke, B. L. Schürmann, and J. P. Rabe, *J. Chem. Phys.* **96**, 6213 (1992).
- ²⁴J. P. Rabe and S. Buchholz, *Phys. Rev. Lett.* **66**, 2096 (1991).
- ²⁵An explicit calculation on a related model in three dimensions shows that, for instance, the nematic phase might be abandoned altogether near the wormlike chain limit (see Ref. 27).
- ²⁶T. J. Sluckin, *Liquid Cryst.* **6**, 111 (1989).
- ²⁷R. Hentschke and J. Herzfeld, *Phys. Rev. A* **44**, 1148 (1991).